

# Forward hadron production in ultra-peripheral proton–heavy-ion collisions at the LHC and RHIC

Gaku Mitsuka <sup>a,1</sup>

<sup>1</sup>Università degli Studi di Firenze and INFN Sezione di Firenze,  
Via Sansone 1, 50019 Sesto Fiorentino (Fi), Italy

March 28, 2022

**Abstract** We present a hadron production study in the forward rapidity region in ultra-peripheral proton–lead ( $p + \text{Pb}$ ) collisions at the LHC and proton–gold ( $p + \text{Au}$ ) collisions at RHIC. The present paper is based on the Monte Carlo simulations of the interactions of a virtual photon emitted by a fast moving nucleus with a proton beam. The simulation consists of two stages: the STARLIGHT event generator simulates the virtual photon flux, which is then coupled to the SOPHIA, DPMJET, and PYTHIA event generators for the simulation of particle production. According to these Monte Carlo simulations, we find large cross sections for ultra-peripheral collisions particle production, especially in the very forward region. We show the rapidity distributions for charged and neutral particles, and the momentum distributions for neutral pions and neutrons at high rapidities. These processes lead to substantial background contributions to the investigations of collective nuclear effects and spin physics. Finally we propose a general method to distinguish between proton–nucleus ( $p + A$ ) inelastic interactions and ultra-peripheral collisions which implements selection cuts based on charged-particles multiplicity at mid-rapidity and/or neutron activity at negative forward rapidity.

## 1 Introduction

High-energy  $p + A$  collisions can be classified into the following two categories depending on the impact parameter  $b$ . In the first category,  $p + A$  collisions occur with geometrical overlap of the colliding proton and nucleus, where the impact parameter is smaller than the sum of the radii of each particle, namely,  $b < R_p + R_A$  ( $R_p$  and  $R_A$  are the radius of the proton and nucleus, respectively.)

In the second category instead, the impact parameter exceeds the sum of the two radii,  $b > R_p + R_A$ , thus there is

no geometrical overlap between the colliding hadrons and hadronic interactions are strongly suppressed. Nevertheless, virtual photons emitted from one of the two colliding hadrons may anyway interact with another hadron. This process is usually referred to as ultra-peripheral collision (UPC, see Ref. [1,2] for a review).

UPCs, so far, have been used for the determination of the gluon distribution in protons and nuclei. For example, photoproduction of quarkonium in ultra-peripheral  $p + A$  collisions can probe a high, or possibly saturated, parton density in protons at small Bjorken- $x$  (i.e., small parton momentum fraction of the momentum of protons). Indeed measurements already exist of exclusive  $J/\psi$  photoproduction at the CERN Large Hadron Collider (LHC), namely,  $p + \text{Pb} \rightarrow p + \text{Pb} + J/\psi$  [3]. Conversely, less attention has been paid, in UPCs, to particle production in general photon–proton interactions, i.e.,  $\gamma + p \rightarrow X$ , but nevertheless such particle production should be considered as well in the investigation of collective nuclear effects. Because a large cross section is expected, this process in UPCs provides significant background events to pure  $p + A$  inelastic interaction events (hereafter “hadronic interaction”, unless otherwise noted) used for such investigations. Indeed, a sizable cross section was found for hadron production in ultra-peripheral  $d + \text{Au}$  collisions [4], which amounted to  $\sim 10\%$  of the  $d + \text{Au}$  inelastic cross section. However, in Ref. [4], only the cross section for UPCs was presented, and the discussion of the rapidity and momentum distributions of the UPC induced events was unfortunately neglected.

In this paper, we discuss the effects of particle production by  $\gamma + p$  interaction in ultra-peripheral  $p + A$  collisions compared to the measurements of hadronic interactions in terms of the rapidity and momentum distributions, especially in forward rapidity regions at the LHC and the BNL Relativistic Heavy Ion Collider (RHIC). Concerning  $p + \text{Pb}$  collisions at  $\sqrt{s_{NN}} = 5.02 \text{ TeV}$  at the LHC, we perform the calcula-

<sup>a</sup>e-mail: gaku.mitsuka@cern.ch

tions assuming that the measurements of  $\pi^0$ s and neutrons are made with zero-degree calorimeters (ZDCs, for example, the ATLAS-ZDCs [5]) and the LHCf detector [6], which are capable of investigating nuclear effects using hadronic interaction events in the very forward region. For the case at RHIC, we consider the  $\pi^0$  and neutron measurements in  $p + \text{Au}$  collisions at  $\sqrt{s_{NN}} = 200 \text{ GeV}$  in the year 2015. The STAR and PHENIX experiments propose a study on partonic processes in nuclei using forward prompt photons, where decay photons from  $\pi^0$ s (from both the hadronic interaction and UPCs) would be the dominant background events [7, 8]. Furthermore, measurements of the hadronic-interaction-induced prompt photons and  $\pi^0$ s in transversely polarized  $p + \text{Au}$  collisions may provide key information on the yet unestablished contributions of Sivers and Collins effects to the single spin asymmetry [7, 8].

Our quantitative discussions on forward hadron production are based on Monte Carlo (MC) simulations. The MC simulation for UPCs consists of two steps; the virtual photon flux is simulated by the STARLIGHT event generator [9, 10] and then the subsequent particle production in  $\gamma + p$  interactions is simulated by the SOPHIA [11, 12], DPMJET [13, 14], and PYTHIA [15, 16] event generators. STARLIGHT in this study has been partially customized in order to transfer the information on the simulated virtual photon to SOPHIA. The MC simulation for hadronic interactions is performed by the DPMJET alone.

The paper is organized as follows. First, in Sect. 2, the methodology of the MC simulations is explained. Next, in Sect. 3, we discuss the simulation results in terms of the rapidity and momentum distributions, where the hadron production in UPCs is compared to that in hadronic interactions. Additionally, we attempt a reduction in UPC events by requiring associated particles. Conclusions are drawn in the last section. In this paper natural units  $\hbar = c = 1$  are used throughout.

## 2 Monte Carlo simulations Methodology

As stated above, the MC simulation for UPCs in this study consists of two steps. First, we simulate the virtual photon flux as a function of the photon energy and impact parameter by using STARLIGHT [9]. Next, the simulation of the  $\gamma + p$  interaction is performed by using SOPHIA [11] at low energy and either DPMJET [13] or PYTHIA [15] at high energy. The methodology of the MC simulation for UPCs is explained in the following subsections from 2.1 to 2.3. In these subsections, the proton rest frame is referenced to unless otherwise noted. The MC simulation for hadronic interactions is simply performed by using DPMJET, and will be described in Sect. 2.4.

### 2.1 Virtual photon flux simulation

In this paper, the energy spectrum of the virtual photons emitted by the relativistic nucleus follows the Weizsäcker-Williams approximation [17, 18] implemented in STARLIGHT. The double differential photon flux due to the fast moving nucleus with velocity  $\beta$  is written as

$$\frac{d^3N}{dE_\gamma db^2} = \frac{Z^2 \alpha}{\pi^2} \frac{x^2}{E_\gamma b^2} \left( K_1^2(x) + \frac{1}{\gamma^2} K_0^2(x) \right), \quad (1)$$

where  $N$  is the number of the emitted photons,  $E_\gamma$  is the photon energy,  $Z$  is the electric charge ( $Z = 82$  for Pb and  $Z = 79$  for Au),  $\alpha$  is the fine structure constant,  $x = E_\gamma b / \gamma$  ( $\gamma = \sqrt{1 - \beta^2}^{-1/2}$  is the Lorentz factor), and  $K_0$  and  $K_1$  are the modified Bessel functions. In the case of a relativistic nucleus ( $\gamma \gg 1$ ), the contribution of the term  $K_0^2(x) / \gamma^2$  in Eq. (1) can be safely disregarded, and in fact STARLIGHT considers only the term  $K_1^2(x)$ . For heavy nuclei with a large radius, the virtuality of the photon  $|q^2| < (1/R_A)^2$  can be neglected. Thus all photons are treated as real photons in the simulation for this analysis. Another approximation is due to the fact that here we assume a point charge for the nucleus and this assumptions may lead to a certain level of systematic uncertainty. For example, as discussed in Ref. [19], the photon flux in reality depends on the choice of the form factor in the nucleus by  $\lesssim 20\%$ .

The probability  $P_{\text{UPC}(\gamma+p \rightarrow X)}(b)$  for a single photon interaction with a proton in UPCs as a function of  $b$  is given by

$$P_{\text{UPC}(\gamma+p \rightarrow X)}(b) = \int_{E_\gamma^{\min}}^{E_\gamma^{\max}} \frac{d^3N}{dE_\gamma db^2} \sigma_{\gamma+p \rightarrow X}(E_\gamma) \overline{P}_{\text{had}}(b) dE_\gamma \quad (2)$$

where  $\sigma_{\gamma+p \rightarrow X}(E_\gamma)$  is the total cross section for a single real photon interaction with a rest proton and  $\overline{P}_{\text{had}}(b)$  is the probability of having no hadronic interactions in  $p + A$  collisions.  $E_\gamma^{\min}$  and  $E_\gamma^{\max}$  are the minimum and maximum photon energies.

In this study, we take  $\sigma_{\gamma+p \rightarrow X}(E_\gamma)$  from the compilation of present experimental results [20] when a photon-proton center-of-mass energy  $W_{\gamma+p}$  is smaller than 7 GeV. A linear interpolation is performed between each data point. The cross section at the exact photopion production threshold,  $E_\gamma = 0.15 \text{ GeV}$ , for which no experimental measurement exists, is forced to zero. At  $W_{\gamma+p}$  larger than 7 GeV,  $\sigma_{\gamma+p \rightarrow X}(E_\gamma)$  is derived from the best COMPETE fit results [20].

A finite probability for having no hadronic interactions  $\overline{P}_{\text{had}}(b)$  is introduced in order to implement a smooth cut off for values of the impact parameter approaching:  $b = R_p + R_A$ .  $\overline{P}_{\text{had}}(b)$  is calculated from the Woods-Saxon nuclear density and the Glauber model [9].

The range of the impact parameter  $b$  considered in the simulation extends from  $b^{\min} = 4$  fm to  $b^{\max} = 10^5$  fm.  $b^{\min}$  is well below the sum of the effective radii of colliding particles ( $\sim 8$  fm for both  $p + \text{Pb}$  and  $p + \text{Au}$  collisions), and  $\overline{P}_{\text{had}}(b)$  rapidly approaches zero below 8 fm. The photon energy  $E_\gamma$  in the simulation ranges from slightly above the photopion production threshold, i.e.,  $E_\gamma^{\min} = 0.16$  GeV, to  $E_\gamma^{\max}$ .  $E_\gamma^{\max}$  is obtained from  $\gamma/b^{\min}$  and amounts to 700 TeV for  $p + \text{Pb}$  collisions at LHC and 1.1 TeV for  $p + \text{Au}$  collisions at RHIC.

## 2.2 Simulation of the low-energy photon–proton interaction

The particle production from the interaction of a low-energy photon with a proton is simulated by the SOPHIA 2.1 event generator [11]. In SOPHIA, particle production via baryon resonances, direct pion production, and multiparticle production are taken into account. For the baryon resonances, the known resonances from  $\Delta(1232)$  to  $\Delta(1950)$  are considered with their physical parameters. The resonance decays isotropically, depending on the available phase space. The non-diffractive interaction, which is implemented using the dual parton model [21], starts to dominate at  $E_\gamma \gtrsim 2$  GeV increasing with energy. The diffractive interaction is implemented as the quasi-elastic exchange of a reggeon or pomeron between virtual hadronic states of the photon and the proton. The SOPHIA generator is used for the UPC simulations, with the photon energy ranging from  $E_\gamma^{\min}$  to  $E_\gamma^{\text{cut}}$ .  $E_\gamma^{\text{cut}}$  is a "technical" cut off energy that distinguishes low energy from high-energy interactions for SOPHIA and the other generators.

Here we emphasize that, firstly, the simulation with the photon energy  $E_\gamma \lesssim 0.5$  GeV is crucial for producing low transverse-momentum ( $p_T$ ) UPC induced events that are dominant in the very forward regions of the detector reference frame (explained in Sect. 3.3), secondly, SOPHIA can simulate the interaction of such a low-energy photon with a proton above the photopion production threshold, and, finally, a newly developed interface to SOPHIA has been introduced into STARLIGHT that was not originally coupled to SOPHIA. This interface provides two main functions: first, the information on the simulated photon by STARLIGHT is transferred to SOPHIA, and second, the information on the produced particles after the simulation of the  $\gamma + p$  interaction are returned from SOPHIA to STARLIGHT for, e.g., Lorentz boost, listing of the produced particles, etc.

## 2.3 Simulation of high-energy photon–proton interaction

At the photon energy  $E_\gamma > E_\gamma^{\text{cut}}$ , we perform the simulation of  $\gamma + p$  interactions by using either PYTHIA 6.428 or DPMJET 3.05. STARLIGHT has its own interface to both event generators.

**Table 1** Summary of the event generators for  $\gamma + p$  interactions and their cut off energies. "Low-energy" and "High-energy" in the table indicate the energy regions  $E_\gamma^{\min} < E_\gamma < E_\gamma^{\text{cut}}$  and  $E_\gamma^{\text{cut}} < E_\gamma < E_\gamma^{\max}$ , respectively.

	$\gamma + p$ interactions		
	Low-energy	High-energy	$E_\gamma^{\text{cut}}$
SOPHIA+PYTHIA	SOPHIA 2.1	PYTHIA 6.428	55 GeV
SOPHIA+DPMJET	SOPHIA 2.1	DPMJET 3.05	6 GeV

In PYTHIA [15], the high-energy photon interactions with a proton are classified into three different schemes [22]. Direct events describe the bare photon interaction with a parton from the proton, typically leading to high  $p_T$  jets. In vector meson dominance (VMD) events, the photon fluctuates into a vector meson and then the vector meson interacts with the proton. This class includes low- $p_T$  events. Finally, generalized VMD events are where the photon fluctuates into a  $q\bar{q}$  pair which interacts with a parton from the proton. Single photon dissociation and single proton dissociation occur in the relatively low  $p_T$  region. PYTHIA requires a simulated event that has a center-of-mass energy  $W_{\gamma+p}$  larger than 10 GeV. This energy corresponds to a photon energy  $E_\gamma = 55$  GeV. Thus SOPHIA and PYTHIA are employed for the simulation of a  $\gamma + p$  interaction for photon energies below and above  $E_\gamma^{\text{cut,PYTHIA}} = 55$  GeV, respectively.

DPMJET [13] is based on the two-component dual parton model.  $\gamma + p$  interactions are especially implemented in the PHOJET MC event generator [23] inside DPMJET. In PHOJET, the physical photon is described as a superposition of the bare photon and virtual hadronic photon. The bare photon directly interacts with partons from the proton. The virtual hadronic photon first fluctuates into a  $q\bar{q}$  pair and then hadronically interacts with the proton. Both single photon dissociation and single proton dissociation are also taken into account. DPMJET requires  $E_\gamma^{\text{cut,DPMJET}} \geq 6$  GeV, the lowest energy that guarantees usable results from the model. Thus, SOPHIA and DPMJET are employed for the simulation of a  $\gamma + p$  interaction for photon energies below and above 6 GeV, respectively.

As summarized in Table 1, we have thus two types of UPC simulations: the first one given by the simulations of photohadron production performed by SOPHIA and PYTHIA with a cut off energy of  $E_\gamma^{\text{cut,PYTHIA}} = 55$  GeV, the second one deriving from simulations performed by SOPHIA and DPMJET with  $E_\gamma^{\text{cut,DPMJET}} = 6$  GeV.

## 2.4 Simulation of hadronic interactions

In this paper, DPMJET is used as an event generator for the MC simulation of hadronic interactions, which include non-diffractive and diffractive interactions but do not include

elastic scattering. The multiple scattering process in the interaction with a nuclear target, which causes nuclear shadowing, is described by the Gribov-Glauber model [24, 25] in terms of the multiple pomeron exchange. Some of the parameters for soft particle production are set at the values that best reproduce experimental results. The integrated interface CRMC 1.5.3 [26] is used to access the DPMJET generator.

### 3 Predictions for ultra-peripheral collisions at LHC and RHIC

#### 3.1 Total cross sections

The total cross section for UPCs ( $\sigma_{\text{UPC}(\gamma+p \rightarrow X)}$ ) is calculated by integrating Eq. (2) over the parameter  $b$ :

$$\begin{aligned} \sigma_{\text{UPC}(\gamma+p \rightarrow X)} &= \int_{b^{\min}}^{b^{\max}} P_{\text{UPC}(\gamma+p \rightarrow X)} db^2 \\ &= 2\pi \int_{b^{\min}}^{b^{\max}} \int_{E_{\gamma}^{\min}}^{E_{\gamma}^{\max}} \frac{d^3N}{dE_{\gamma} db^2} \sigma_{\gamma+p \rightarrow X}(E_{\gamma}) \\ &\quad \times \overline{P}_{\text{had}}(b) b db dE_{\gamma}. \end{aligned} \quad (3)$$

As discussed in Sect. 2.1, Eq. (1) and  $\overline{P}_{\text{had}}(b)$  are obtained by using STARLIGHT, while  $\sigma_{\gamma+p \rightarrow X}(E_{\gamma})$  is taken from experimental measurements and best fit results to these measurements; thus, Eq. (3) is independent from the other event generators: SOPHIA, DPMJET, and PYTHIA. The calculated cross sections  $\sigma_{\text{UPC}(\gamma+p \rightarrow X)}$  at the LHC and RHIC are summarized in Table 2. The cross sections for  $p+A$  inelastic interactions, calculated by using DPMJET, are also presented. We find a sizable  $\sigma_{\text{UPC}(\gamma+p \rightarrow X)}$ s, which amount to 20% and 9% of the hadronic cross sections at the LHC and RHIC respectively. Effective cross sections that require forward  $\pi^0$  and neutron tagging will be discussed later in Sect. 3.3.

For reference we have computed the cross section in ultra-peripheral  $d+Au$  collisions at  $\sqrt{s_{NN}} = 200$  GeV in the same manner as Eq. (3) and using the same photon energy and impact parameter ranges as in Ref. [4], obtaining a  $\sigma_{\text{UPC}(\gamma+d \rightarrow X)} = 230$  mb, which is compatible with the result obtained by Ref. [4]. Since the photon energy and impact parameter ranges used for the comparison are narrower than the ranges used in the computation of Table 2, the cross section  $\sigma_{\text{UPC}(\gamma+d \rightarrow X)}$  is smaller than twice the cross section  $\sigma_{\text{UPC}(\gamma+p \rightarrow X)}$  in Table 2, namely,  $2\sigma_{\text{UPC}(\gamma+p \rightarrow X)} = 340$  mb. The factor of 2 comes from  $\sigma_{\gamma+d \rightarrow X}(E_{\gamma}) \approx 2\sigma_{\gamma+p \rightarrow X}(E_{\gamma})$ .

Now, to have a comparison with  $\sigma_{\text{UPC}(\gamma+p \rightarrow X)}$ , we have also calculated the cross section  $\sigma_{\text{UPC}(\gamma+A \rightarrow X)}$  for UPCs where a photon emitted by a fast moving proton interacts with a nucleus  $A$  ( $A$  is either Pb or Au), although this process is not taken into account in the MC simulations performed for this study. In ultra-peripheral  $p+A$  collisions, the number of photons emitted by the proton is generally smaller than

that by the nucleus due to the  $Z^2$  dependence. The interactions of a single real photon with a nucleus can be roughly classified into two categories in terms of the photon energy in the nucleus rest frame, namely below or above the photopion production threshold. For  $7 \text{ MeV} < E_{\gamma} < 140 \text{ MeV}$ , thus below the photopion production threshold, the cross sections for photonuclear absorption processes are studied for Pb and Au nuclei in Ref. [27, 28]. Here a certain number of neutrons are emitted from the decay of the photoexcited nucleus in the event, in particular at least one neutron is emitted almost 100% of the time. For  $E_{\gamma} > 140 \text{ MeV}$ , the  $\gamma+A$  cross section can be calculated within the Gribov-Glauber approximation [29]. The calculated  $\gamma+A$  cross section  $\sigma_{\gamma+A \rightarrow X}(E_{\gamma})$  is compatible with or smaller than the simply scaled  $\gamma+p$  cross section  $(Z+N)\sigma_{\gamma+p \rightarrow X}(E_{\gamma})$  ( $Z$  and  $N$  are the atomic number and neutron number of the nucleus, respectively.) The suppression of  $\sigma_{\gamma+A \rightarrow X}(E_{\gamma})$  relative to  $(Z+N)\sigma_{\gamma+p \rightarrow X}(E_{\gamma})$  appears at  $E_{\gamma} > 2 \text{ GeV}$  because of nuclear shadowing [29]. Consequently, in ultra-peripheral  $p+Au$  and  $p+Pb$  collisions, the process with photon emission from the proton is suppressed with respect to that from the nucleus. The cross section of the former process ( $\sigma_{\text{UPC}(\gamma+A \rightarrow X)}$ ) amounts to 6% of the latter ( $\sigma_{\text{UPC}(\gamma+p \rightarrow X)}$ ).

Since the UPC simulations used in this paper assume that only a single photon is produced from the moving nucleus in any event, UPCs involving two or more photons are not taken into account in the study. However UPC processes with the exchange of two photons between the proton and the nucleus generally have a huge cross section. In particular, the two-photon exchange leading to di-electrons has a cross section  $\sigma_{\text{UPC}(\gamma+\gamma \rightarrow e+e)}$  of  $\sim 29$  b at the LHC and of  $\sim 4$  b at RHIC ( $\propto (Z_p \alpha)^2 (Z_A \alpha)^2$ , where  $Z_p$  and  $Z_A$  are the electric charges of the proton and nucleus, respectively). These cross sections are obtained by scaling the corresponding cross sections in ultra-peripheral Pb+Pb and Au+Au collisions [30, 31] with the ratio of  $(Z_p/Z_A)^2$ , respectively. The two-photon exchange leading to other particle pairs, e.g.,  $\mu^+ \mu^-$ ,  $\tau^+ \tau^-$ , and mesons, are at most  $10^{-3}$  % compared with the di-electron channel [32]. Concerning forward  $\pi^0$  and neutron productions providing background contribution to hadronic interaction events, we consider a higher-order process where the two-photon exchange is accompanied by an additional inelastic interaction of the single photon emitted from the nucleus with the proton. This process can be factorized into two subprocesses: the two-photon exchange and the  $\gamma+p$  interaction [33]. Accordingly, the cross section is calculated using:

$$\begin{aligned} \sigma_{\text{UPC}(\gamma+\gamma \rightarrow e+e, \gamma+p \rightarrow X)} &= \\ &\int_{b^{\min}}^{b^{\max}} P_{\text{UPC}(\gamma+\gamma \rightarrow e+e)}(b) P_{\text{UPC}(\gamma+p \rightarrow X)}(b) db^2, \end{aligned} \quad (4)$$

where  $P_{\text{UPC}(\gamma+\gamma \rightarrow e+e)}(b)$  is the probability for the two-photon exchange leading to di-electron and  $P_{\text{UPC}(\gamma+p \rightarrow X)}(b)$  is the

**Table 2** Cross sections for particle production in ultra-peripheral collisions and hadronic interactions at the LHC and RHIC.

	UPC (mb)			Hadronic interaction (mb)		
	Total	$\pi^0$	$n$	Inelastic	$\pi^0$	$n$
LHC	434	78	153	2189	91	125
RHIC	170	9	73	1851	67	35

probability defined in Eq. (2). With the former probability taken from the results in Refs. [34,35], we obtain  $\sigma_{\text{UPC}}(\gamma+\gamma\rightarrow e+e, \gamma+p\rightarrow X) = 66$  mb at the LHC and 15 mb at RHIC. These cross sections correspond to 15% and 9% compared with  $\sigma_{\text{UPC}}(\gamma+p\rightarrow X)$  shown in Table 2 at the LHC and RHIC, respectively.

### 3.2 Rapidity distributions

The charged and neutral particle pseudorapidity ( $\eta_{\text{lab}}$ ) distributions in the detector reference frame are shown in Fig. 1. The solid curves indicate the UPC simulation events generated by using SOPHIA at low energy and DPMJET at high energy. The dashed curves indicate the UPC simulation events generated by using SOPHIA at low energy and PYTHIA at high energy. The dotted curves indicate the predictions for  $p+Pb$  and  $p+Au$  inelastic events with DPMJET at the LHC and RHIC respectively. Hereafter the directions for the moving proton and nucleus are assumed to have positive and negative rapidities respectively. The directions for both particles are indicated by the arrows in the upper left panel of Fig. 1 ( $p$  for proton and  $A$  for nucleus).

In Fig. 1, the pseudorapidity distributions in hadronic interactions achieve a plateau at mid-rapidity and also have a large number of spectator nucleons at  $\eta_{\text{lab}} \sim -8$ . Conversely, particle production in UPCs is clearly clustered around positive forward rapidities, since the UPC induced events in this study are produced only by the interactions of the photon emitted from the nucleus with the proton. It should be noted that the cross sections for UPCs exceed those of hadronic inelastic interactions for charged and neutral particles at  $\eta_{\text{lab}} > 9$  at the LHC and  $\eta_{\text{lab}} > 7$  at RHIC. This indicates that contamination from background UPC events, could spoil the investigation of collective nuclear effects and spin physics carried out from measurements of hadronic interactions in those rapidity regions.

### 3.3 Transverse and longitudinal momentum distributions

The simulated  $p_T$  and longitudinal momentum fraction ( $z$ , defined as  $p_z/p_{z,\text{max}}$ ) distributions for  $\pi^0$ s and neutrons at positive forward rapidities (direction of the proton remnant), are shown in Fig. 2 for the LHC and in Fig. 3 for RHIC. For the distributions at the LHC, we chose rapidity

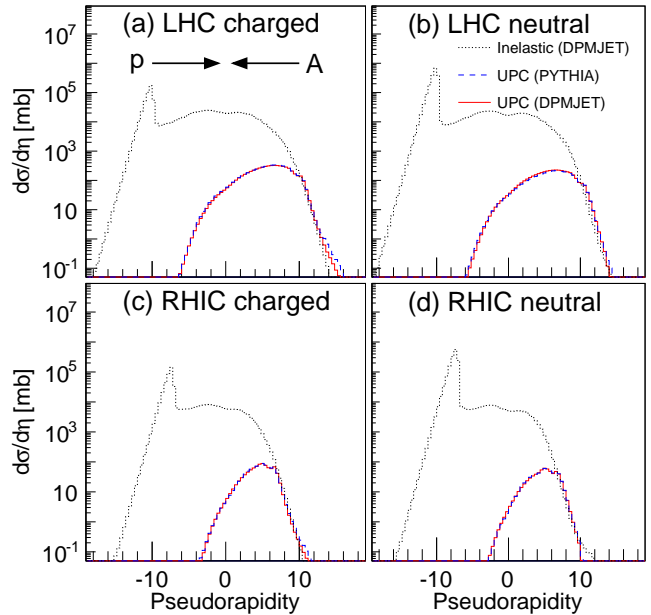


**Fig. 1** Charged (left) and neutral particle (right) pseudorapidity distributions at the LHC (top) and RHIC (bottom), respectively. The solid curves and dashed curves indicate the UPC simulation events generated by using STARLIGHT+SOPHIA+DPMJET and STARLIGHT+SOPHIA+PYTHIA, respectively. The dotted curves indicate the simulated  $p+Pb$  and  $p+Au$  inelastic events with DPMJET at the LHC and RHIC, respectively. The directions of the moving proton ( $p$ ) and the nucleus ( $A$ ) are indicated by arrows in the upper left panel.

regions in the detector reference frame  $8.5 < y_{\text{lab}} < 11.0$  for  $\pi^0$ s and  $7.0 < y_{\text{lab}} < 9.05$  for neutrons, which roughly correspond to the acceptances of the ATLAS-ZDCs [5] and LHCf detector [6]. These detectors provide an opportunity to investigate the effects of high parton density on forward  $\pi^0$ s and neutrons, which emerge as a suppression in the momentum distributions in  $p+Pb$  inelastic interactions relative to that of  $p+p$  inelastic interactions.

In the upper left and bottom left panels of Fig. 2, the  $p_T$  distributions of  $\pi^0$ s and neutrons in UPCs show a steep peak at  $p_T \approx 0.2$  GeV. These peaks originate from the  $\gamma+p \rightarrow \pi^0+p$  and  $\gamma+p \rightarrow \pi^++n$  channels, via baryon resonances. In fact, in the proton rest frame the  $\gamma+p$  interactions, with a photon energy ranging from  $E_{\gamma}^{\text{min}}$  to 0.5 GeV, have a center-of-mass energy of  $1.1 < W_{\gamma+p} < 1.3$  GeV and thus occur in the baryon resonance region, which has a larger cross section compared to other energy regions. Conversely, the  $\gamma+p$  interactions with higher photon energies are suppressed due to a decrease in the photon flux with increasing photon energy. Therefore the  $\pi^0$ s and neutrons emitted by the decay of the baryon resonances due to low-energy  $\gamma+p$  interactions (dominantly  $\Delta^+(1232)$ ) which typically have  $p_T \approx 0.2$  GeV provide substantial contributions to the  $p_T$  distributions of each particle. Thus, the double differential UPC cross sections exceed those of hadronic interactions for  $p_T \approx 0.2$  GeV. The dominance of the  $\gamma+p \rightarrow \pi^++n$

channel in UPCs is also evident in the bottom right panel of Fig. 2. Forward neutrons produced in UPCs have a larger  $z$  value; low momentum neutrons produced by a low-energy  $\gamma + p$  interaction in the proton rest frame are boosted to nearly the same velocity of the projectile proton. Finally, we see that the presence of UPCs certainly provides a significant background contribution to the study of collective nuclear effects.

The  $p_T$  and  $z$  distributions for  $\pi^0$ s and neutrons produced at RHIC are shown in Fig. 3. We chose the rapidity regions  $3.1 < y_{\text{lab}} < 3.8$  for  $\pi^0$ s and  $4.0 < y_{\text{lab}} < 5.4$  for neutrons, which correspond to the acceptance of the MPC-EX detector [8] and ZDC [36] of the PHENIX experiment respectively. Since these rapidity regions are near the acceptance of the FMS+pre-shower detector [7] and ZDC [36] of the STAR experiment, the following discussion is essentially applicable also to measurements performed at the STAR experiment. The prompt photon measurements in  $p + \text{Au}$  collisions with the MPC-EX detector in PHENIX and the FMS+pre-shower detector in STAR could provide key information on partonic processes in the Au nucleus, whereas photons from  $\pi^0$ s decays, produced both from hadronic interactions and UPCs, could be the dominant background events. The  $p_T$  distributions of  $\pi^0$ s from UPCs have almost the same shapes as those coming from hadronic interactions (the upper left panel), while the absolute yield is at most 3% of that of hadronic interactions. Thus, we conclude that UPCs provide a negligible contribution to the amount of  $\pi^0$ s giving background photon events. The  $z$  distribution of  $\pi^0$ s from UPCs (the upper right panel) is slightly steeper than for hadronic interactions, but the absolute yield is once again negligible. On the other hand, neutrons produced in UPCs compete with those from hadronic interactions at  $p_T \lesssim 0.2 \text{ GeV}$ . This can be explained by the same mechanism found in Fig. 2, namely dominance of the  $\gamma + p \rightarrow \pi^+ + n$  channel via baryon resonances in UPCs. The  $z$  distribution of neutrons has a similar shape to that shown in the bottom right panel of Fig. 2. Concerning the measurements of forward prompt photons,  $\pi^0$ s, and neutrons in polarized  $p + \text{Au}$  collisions, which are sensitive to the origin of spin asymmetry [37], we confirm that the UPC contribution to the total number of prompt photons and  $\pi^0$ s is negligible, while neutrons instead, are produced in similar amounts from both UPCs and hadronic interactions.

We need to test now, both for the LHC and RHIC simulations, a possible dependence of the  $p_T$  and  $z$  distributions on the cut off energy  $E_\gamma^{\text{cut}}$  that was introduced in Sect. 2.2 and 2.3. The comparison of the two distributions at the LHC, with one based on the UPC simulations with DPMJET above  $E_\gamma^{\text{cut,DPMJET}} = 6 \text{ GeV}$  and the other based on the UPC simulations with DPMJET above  $E_\gamma^{\text{cut,DPMJET}} = 55 \text{ GeV}$ , shows a negligible difference between these two. The comparison in the RHIC case shows larger differences than at LHC; nevertheless they are at the same level of those between DPMJET

and PYTHIA. There is also a significant difference for the  $p_T$  distributions of neutrons at the LHC between DPMJET and PYTHIA (the bottom left panel of Fig. 2); PYTHIA predicts a harder spectrum and has  $\sim 8$  times larger number of neutrons at  $p_T \approx 2 \text{ GeV}$  than DPMJET. This difference is mostly caused by a strong dependence of the multiplicity of leading baryons on the minimum  $p_T$  ( $p_{T\text{min}}$ ) for the multiple interactions (i.e., hard scattering) implemented by each model. In general, a lower  $p_{T\text{min}}$  provides more multiple interactions in an event which then leads to a higher multiplicity. Changing the  $p_{T\text{min}}$  value in PYTHIA (PARP(81), 1.9 GeV as a default) to the default value of DPMJET (2.5 GeV) significantly modifies the  $p_T$  distribution in PYTHIA bringing an overall agreement between the two.

Looking back at Table 2 we see that the effective cross sections for  $\pi^0$  and neutron productions are defined as the cross sections having at least one  $\pi^0$  or neutron hitting within the rapidity ranges highlighted above. We find that UPC cross sections are similar or larger than the hadronic cross sections, except for the  $\pi^0$  one at RHIC. It should be noted that the effective cross section estimation involves simulations of specific hadron productions and is thus no longer independent of the generators used for hadronic interactions. The values in Table 2 for UPCs are calculated by using STARLIGHT, SOPHIA, and DPMJET, and those for hadronic interactions are calculated by using DPMJET. Nevertheless, the essence of our conclusions will not depend on the choice of event generators.

Finally, we roughly estimate the contribution to UPCs where the proton acts as the photon source, which was not taken into account in the MC simulation of this paper, and the possible changes to the  $p_T$  and  $z$  distributions. Because of the directions of the colliding photon and nucleus and because of the smaller cross sections (calculated in Sect. 3.1), the number of  $\pi^0$ s and neutrons produced at  $y_{\text{lab}} > 3$  is negligible compared with that from UPCs where the nucleus acts as the photon source. Conversely, the two-photon exchange process followed by the  $\gamma + p$  interaction, currently not implemented in the MC simulation as well, would yield  $\pi^0$ s and neutrons at positive forward rapidities amounting to 15% of those shown in Fig. 2 at the LHC and to 9% of those shown in Fig. 3 at RHIC. A more detailed study would need to take two-photon and di-electron interactions into account in the MC simulation framework and is thus beyond the scope of the present paper.

### 3.4 Reduction of ultra-peripheral collisions contributions

As seen in Fig. 1, particle production in UPCs is clustered at positive forward rapidity regions, whereas those in hadronic interactions show a plateau at mid-rapidity and have also a large number of spectator nucleons at  $\eta_{\text{lab}} \sim -8$ . In this section, we present the two methods to separate UPCs

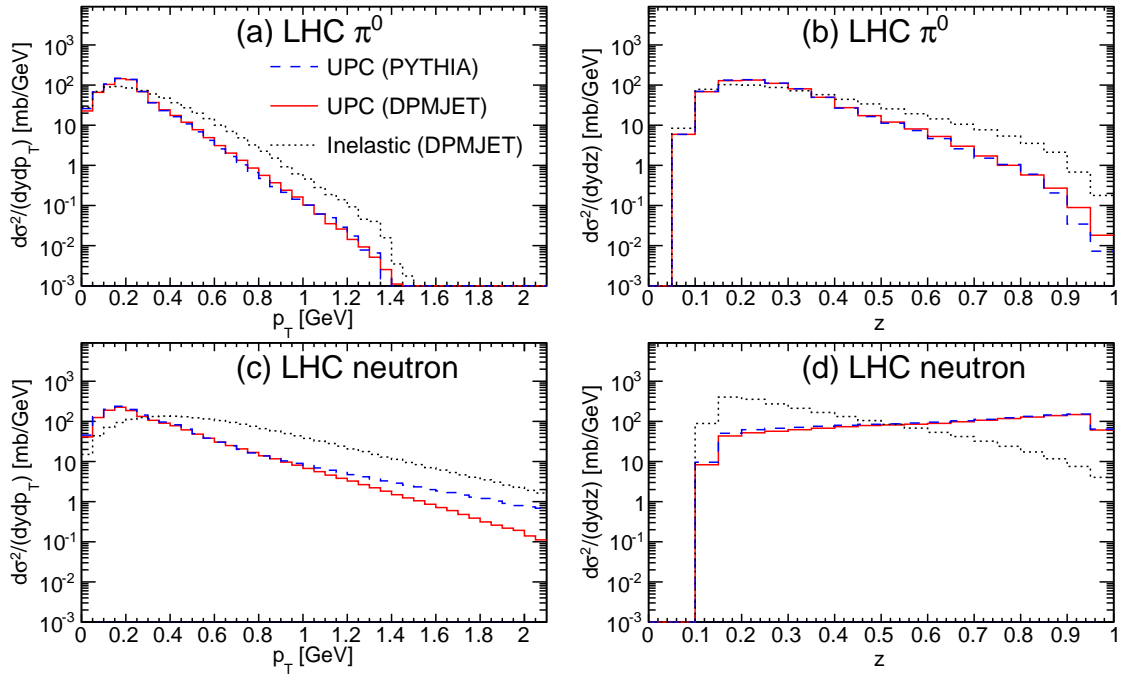


**Fig. 2** Simulated  $p_T$  and  $z$  spectra for  $\pi^0$ s and neutrons in  $p + \text{Pb}$  collisions at the LHC. The solid curves and dashed curves indicate the UPC simulation events generated by using STARLIGHT+SOPHIA+DPMJET and STARLIGHT+SOPHIA+PYTHIA, respectively. The dotted curves indicate the simulated  $p + \text{Pb}$  inelastic events with DPMJET.

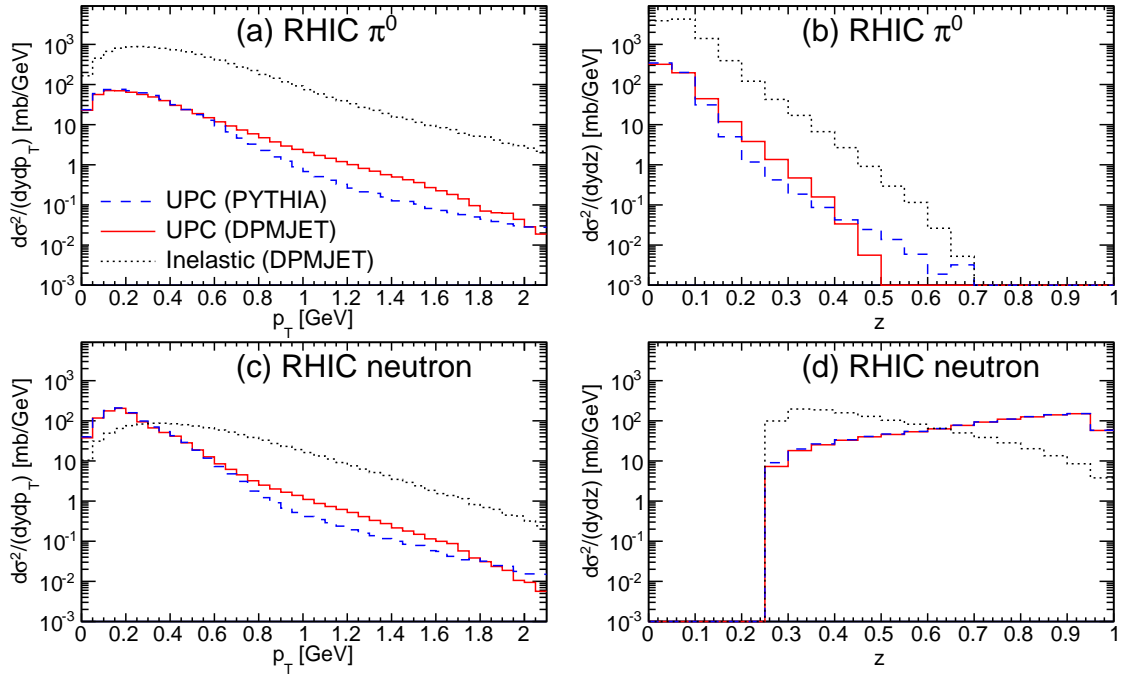


**Fig. 3** Simulated  $p_T$  and  $z$  spectra for  $\pi^0$ s and neutrons in  $p + \text{Au}$  collisions at RHIC. The solid curves and dashed curves indicate the UPC simulation events generated by using STARLIGHT+SOPHIA+DPMJET and STARLIGHT+SOPHIA+PYTHIA, respectively. The dotted curves indicate the simulated  $p + \text{Au}$  inelastic events with DPMJET.

and hadronic interactions by exploiting those differences in the rapidity distributions.

First, we investigate the effects of requiring some activities in the mid-rapidity region. The following cuts are applied to inclusive  $\pi^0$  and neutron measurements to eliminate UPC induced events as well as to ensure that the hadronic interaction events remain unchanged: (1) the number of charged particles should be greater than 2, (2) the charged particles should have  $p_T > 0.2 \text{ GeV}$ , and (3) the charged particles should have rapidity  $|\eta_{\text{lab}}| < 2.5$  at the LHC and  $|\eta_{\text{lab}}| < 0.35$  at RHIC. The rapidity regions used in the cuts correspond to the rapidity ranges of the ATLAS and PHENIX inner detectors [38,39].

Figure 4 shows the  $p_T$  distributions after the cuts at the LHC and RHIC. The absolute yields of UPCs at the LHC (RHIC) are reduced to less than 60% (8%) for  $\pi^0$ s and 40% (10%) for neutrons, even though the absolute yields of hadronic interactions are kept to be larger than, at most, 85% (50%) for  $\pi^0$ s and 85% (20%) for neutrons. Thus these cuts on the charged particles at mid-rapidity reduce the relative yields of UPCs to hadronic interactions by, at most, 15% (0.2%) for  $\pi^0$ s and 25% (1.5%) for neutrons. However the cuts still leave a remnant contribution from UPCs and unavoidably reduce hadronic interaction events. It should also be noted that the rejected hadronic interaction events are mostly single and double diffractive events, generally characterized by a small number of charged particles at mid-rapidity, and that the reduction efficiency of 10%–50% highly depends on forward  $\pi^0$  and neutron energies.

Next, we test sharper cuts, which require an activity in the negative very forward region, i.e., the direction of the nucleus remnant, and which can be tagged by a ZDC. In this rapidity region, only hadronic interactions produce a large number of spectator nucleons fragmented from the colliding nucleus. Each nucleon has an approximate energy of 1.58 TeV at the LHC and 100 GeV at RHIC. The cuts applied to the simulated events consist of three requirements: (1) the number of neutrons should be greater than 1 (note that a proton can be swept away by the magnets located between an interaction point and a detection point, and thus no proton reaches the detector), (2) the neutrons should have  $E > 1 \text{ TeV}$  at the LHC and  $E > 50 \text{ GeV}$  at RHIC, and (3) the neutrons should have a rapidity  $\eta_{\text{lab}} < -6.5$ . The rapidity region  $\eta_{\text{lab}} < -6.5$  roughly corresponds to the acceptance of the ZDC located in the nucleus-going side. As was inferred in Fig. 1, we find that the contribution of UPCs is efficiently eliminated by these cuts, keeping the number of hadronic interactions unchanged.

We conclude that a reduction in the contributions from UPCs to the measurements of forward hadrons is certainly feasible by requiring some activity in mid and forward rapidity regions. In particular, we expect a strong reduction if

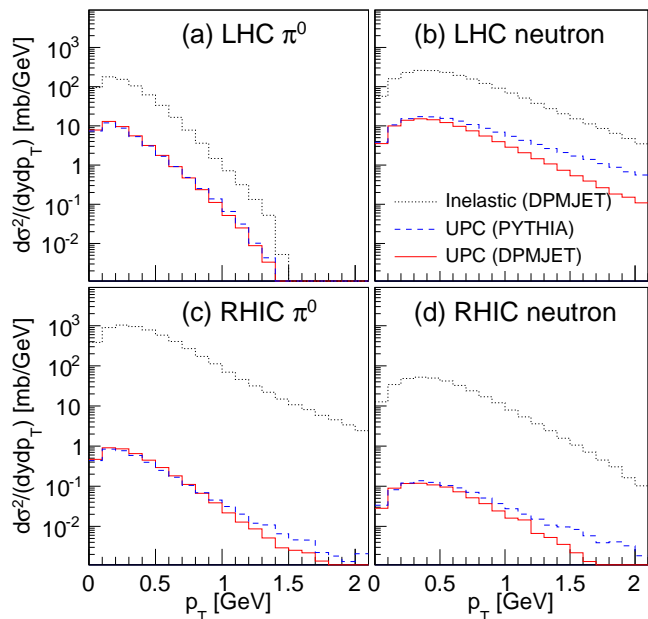


**Fig. 4** Simulated  $p_T$  spectra for  $\pi^0$ s and neutrons with the cuts applied at the LHC and RHIC (see text in detail). The solid curves and dashed curves indicate the UPC simulation events generated by using STARLIGHT+SOPHIA+DPMJET and STARLIGHT+SOPHIA+PYTHIA, respectively. The dotted curves indicate the simulated  $p+A$  inelastic events with DPMJET.

we detect spectator nucleons, for example, with a ZDC, at negative rapidity  $\eta_{\text{lab}} \lesssim -6.5$ .

## 4 Conclusions

Hadron production in forward rapidity regions by ultra-peripheral  $p+Pb$  collisions at the LHC and  $p+Au$  collisions at RHIC was discussed. The present paper was based on MC simulations of the interaction of virtual photons emitted by a fast moving nucleus with a proton, by using several event generators: STARLIGHT, SOPHIA, DPMJET, and PYTHIA. STARLIGHT in this paper was customized in order to transfer the information on the simulated virtual photon to SOPHIA and to receive the information on the produced particles from SOPHIA. This modification made possible the simulation of UPC induced events starting from the photopion production threshold. We found large cross sections for  $\pi^0$  and neutron productions in the very forward region, leading to a substantial background contribution to the measurements of hadronic interactions at both the LHC and RHIC. Therefore, the presence of UPCs had to be taken into account in the analyses focused on the investigation of collective nuclear effects and spin physics, in order to correctly evaluate the fraction of the hadronic cross section relative to the measured cross section. We propose two types of cuts to reduce the fraction of UPCs relative to hadronic interactions; one requires the presence of charged particles at mid-rapidity,

while the other requires the presence of spectator neutrons at negative very forward rapidity. The former cut certainly reduces the UPC induced events while unavoidably rejecting some hadronic events. The second cut efficiently eliminates a fraction of forward  $\pi^0$ s and neutrons produced by UPCs and does not change the number of hadronic interaction events. The proposed methods in this paper were simply based on a tracking detector and a ZDC and thus are generally applicable to the measurements in other experiments that have a similar detector design.

**Acknowledgements** The author would like to thank the authors of STARLIGHT, SOPHIA, PYTHIA, DPMJET, and CRMC for providing the codes of their event generators. The author is also grateful to R. D'Alessandro, K. Kasahara, Y. Muraki, and T. Sako for the useful comments and discussions regarding this topic. The author is supported by the Postdoctoral Fellowships for Research Abroad, Japan Society for the Promotion of Science. Part of this work was performed using the computer resources provided by CERN and INFN-CNAF.

## References

1. C. A. Bertulani and G. Baur, *Phys. Rep.* **163** (1988) 299–408.
2. C. A. Bertulani, S. R. Klein, and J. Nystrand, *Ann. Rev. Nucl. Part. Sci.* **55** (2005) 271–310.
3. ALICE Collaboration, *Phys. Rev. Lett.* **113** (2014) 232504.
4. V. Guzey and M. Strikman, *Phys. Rev. C* **77** (2008) 067901.
5. ATLAS Collaboration, ATLAS Technical Design Report, CERN-LHCC-2007-001 (unpublished).
6. LHCf Collaboration, LHCf Technical Design Report, CERN-LHCC-2006-004 (unpublished).
7. STAR Collaboration, A polarized p+p and p+A program for the next years, STAR Note SN-0605 (2014).
8. PHENIX Collaboration, S. Campbell et al., arXiv:1301.1096.
9. S. R. Klein and J. Nystrand, *Phys. Rev. C* **60** (1999) 014903.
10. STARLIGHT webpage, <https://starlight.hepforge.org/>.
11. A. Mücke, R. Engel, J.P. Rachen, R.J. Protheroe and T. Stanev, *Comput. Phys. Comm.* **124** (2000) 290–314.
12. SOPHIA webpage, <http://homepage.uibk.ac.at/~c705282/SOPHIA.html>.
13. F. W. Bopp, J. Ranft, R. Engel and S. Roesler, *Phys. Rev. C* **77** (2008) 014904.
14. DPMJET webpage, <http://sroesler.web.cern.ch/sroesler/dpmjet3.html>.
15. T. Sjöstrand, S. Mrenna and P. Skands, *JHEP* **05** (2006) 026.
16. PYTHIA 6.4 webpage, <http://pythia6.hepforge.org/>.
17. C. von Weizsäcker, *Z. Physik* **88** (1934) 612–625.
18. E. J. Williams, *Phys. Rev.* **45** (1934) 729–730.
19. M. Kłusek-Gawenda and A. Szczurek, *Phys. Rev. C* **82** (2010) 014904.
20. K. A. Olive et al. (Particle Data Group), *Chin. Phys. C* **38** (2014) 090001.
21. A. Capella, U. Sukhatme, C-I Tan and J. Tran Thanh Van, *Phys. Rep.* **236** (1994) 225–329.
22. G. A. Schuler and T. Sjöstrand, *Phys. Lett. B* **300** (1993) 169–174.
23. R. Engel, *Z. Phys. C* **66** (1995) 203–214.
24. V. N. Gribov, *Sov. Phys. JETP* **30** (1970) 709–717.
25. R. J. Glauber and G. Matthiae, *Nucl. Phys. B* **21** (1970) 135–157.
26. C. Baus, T. Pierog and R. Ulrich, <https://web.ikp.kit.edu/rulrich/crmc.html>.
27. A. Veyssière, H. Beil, R. Bergere, P. Carlos, and A. Leprêtre, *Nucl. Phys. A* **159** (1971) 561–576.
28. A. Leprêtre, H. Beil, R. Bergère, P. Carlos, J. Fagot, A. De Miniac, and A. Veyssière, *Nucl. Phys. A* **367** (1981) 237–268.
29. R. Engel, J. Ranft, and S. Roesler, *Phys. Rev. D* **55** (1997) 6957.
30. D. Yu. Ivanov, A. Schiller, and V. G. Serbo, *Phys. Lett. B* **454** (1999) 155–160.
31. A. J. Baltz, *Phys. Rev. C* **71** (2005) 024901.
32. A. J. Baltz, Y. Gorbunov, S. R. Klein, and J. Nystrand, *Phys. Rev. C* **80** (2009) 044902.
33. K. Hencken, D. Trautmann, and G. Baur, *Z. Phys. C* **68** (1995) 473–479.
34. M. C. Güçlü, J. C. Wells, A. S. Umar, M. R. Strayer, and D. J. Ernst, *Phys. Rev. A* **51** (1995) 1836.
35. K. Hencken, D. Trautmann, and G. Baur, *Phys. Rev. A* **51** (1995) 1874.
36. PHENIX Collaboration, C. Adler et al., *Nucl. Instrum. Meth. A* **470** (2001) 488–499.
37. Z-B Kang and F. Yuan, *Phys. Rev. D* **84** (2011) 034019.
38. ATLAS Collaboration, *JINST* **3** (2008) S08003.
39. PHENIX Collaboration, M. Allen et al., *Nucl. Instrum. Meth. A* **499** (2003) 549–559.